

The Formation of Turbulent Molecular Clouds: A Modeler's View

Fabian Heitsch

Universitäts-Sternwarte München

Scheinerstraße 1

81679 München

heitsch@usm.uni-muenchen.de

Abstract

Molecular Clouds (MCs)- the birth places of stars – are highly structured and “turbulent”. Converging HI flows have been suggested as a possible generation mechanism of molecular clouds, imprinting the observed filamentary structure as a consequence of dynamical and thermal instabilities. I will discuss a numerical analysis of molecular cloud formation via converging HI flows.

Even with modest flow speeds and completely uniform inflows, non-linear density perturbation as possible precursors of MCs arise. Thus, molecular clouds could inevitably be formed with substantial structure, e.g. strong density and velocity fluctuations, which provide the initial conditions for subsequent gravitational collapse and star formation in a variety of galactic and extragalactic environments.

1 Introduction

Molecular clouds (MCs) in our Galaxy are highly structured. With ever increasing observational resolution, the internal structure extends down to the smallest observable scales, possibly even in a self-similar manner (e.g. Elmegreen & Falgarone 1996, Stutzki et al. 1998). Filaments (or sheets) are an ever-reoccurring theme in the morphologies of MCs, on the smaller scales complemented by clumps. The underlying density perturbations are non-linear. Together with the observed non-thermal line-widths (e.g. Falgarone & Philips 1990, Williams et al. 2000), there is strong evidence that MCs are highly dynamical, and very likely not static entities defined by an equilibrium state.

The non-thermal line-widths are generally interpreted as turbulence, i.e. random gas motions within the MCs. Since the line-widths indicate non-thermal velocities of approx. $1 - 2 \text{ km s}^{-1}$, the turbulence would be supersonic with respect to the cold

gas, which has temperatures of about 10 K. The source of this turbulence is unclear (for a summary of the discussion, see Mac Low & Klessen 2004, and Elmegreen & Scalo 2004).

The role of turbulence in molecular clouds is twofold: On the one hand, it has been invoked as a stabilization mechanism for molecular clouds against gravitational collapse, allowing the MC to survive for considerably longer than its freefall time of approximately 1 Myr. However, there is ample evidence from numerical simulations that turbulence decays within a dynamical time scale. Thus, if the turbulence is supposed to support the cloud, it would have to be constantly driven. The second effect of turbulence opposes the support: Due to the shock compressions of the supersonic turbulence, the gas will locally be destabilized against gravitation, so that turbulence would locally even promote collapse (see Mac Low & Klessen 2004).

If the MC needs to be supported by turbulence for much longer than its freefall time, an energy source is required. Most of the suggested mechanisms share one thing in common: Once the cold gas has formed, it is difficult to drive turbulence externally (see e.g. Balsara 1996; Heitsch & Burkert 2002).

An alternative would be to envisage molecular clouds not as well-defined entities in an equilibrium state, but as transient objects forming in a background (HI) flow. This entails that the MC's properties are a consequence of its formation process. The importance of initial conditions for cloud structure and – since the MCs host star forming regions – for star formation is emphasized by observational and theoretical evidence for short cloud “lifetimes” (Ballesteros-Paredes et al. 1999, Elmegreen 2000, Hartmann et al. 2001, Hartmann 2002).

Flows are ubiquitous in the interstellar medium (ISM) due to the energy input by stars – photoionization, winds, and supernovae. In principle, they can pile up atomic gas to form MCs. Shock waves propagating into the warm ISM will fragment in the presence of thermal instability and linear perturbations (Koyama & Inutsuka 2000, 2002, 2004, Hennebelle & Perault 1999, 2000) and allow H₂-formation within a few Myrs (Bergin et al. 2004) in a plane-parallel geometry. We envisage the colliding flows less as e.g. interacting shells, but as (more or less) coherent gas streams from turbulent motions on scales of the order of the Galactic gaseous disk height (Ballesteros-Paredes et al. 1999, Hartmann et al. 2001). Parametrizing the inflows as a ram pressure allowed Hennebelle et al. (2003, 2004) to study the fragmentation and collapse of an externally pressurized slab.

We present a study of the generation of filaments and turbulence in atomic clouds – which may be precursors of MCs – as a consequence of their formation process, extending the model of large-scale colliding HI-flows outlined by Ballesteros-Paredes et al. (1999) and Burkert (2004), see also Audit & Hennebelle (2005). We discuss the dominant dynamical and thermal instabilities leading to turbulent flows and fragmentation of an initially completely uniform flow. Resulting non-thermal linewidths in the cold gas (the progenitors of MCs) reproduce observed values, emphasizing the ease with which turbulent and filamentary structures can be formed in the ISM.

2 Physical Mechanisms

We restricted the models to hydrodynamics including thermal instabilities, leaving out the effects of gravity and magnetic fields. We neglect gravity not because it is not important for the systems considered, but to isolate the effects of the physical mechanisms at work. On the contrary, gravity would lead to further fragmentation on small scales, while on large scales, it could affect the global stability of the cloud. Magnetic fields could have a stabilizing effect especially against shear flows.

For this regime, then, we identify three relevant instabilities:

(1) The Non-linear Thin Shell Instability (NTSI, Vishniac 1994) arises in a shock-bounded slab, when ripples in a two-dimensional slab focus incoming shocked material and produce density fluctuations. The growth rate is $\sim c_s k (k\Delta)^{1/2}$, where c_s is the sound speed, k is the wave number along the slab, and Δ is the amplitude of the spatial perturbation of the slab. Numerical studies focused on the generation of substructure via Kelvin-Helmholtz-modes (Blondin & Marks 1996), on the role of gravity (Hunter et al. 1986) and on the effect of the cooling strength (Hueckstaedt 2003). Walder & Folini (1998, 2000) discussed the interaction of stellar winds, and Klein et al. (1998) investigated cloud collisions. The latter authors included magnetic fields, albeit only partially.

(2) The flows deflected at the slab will cause Kelvin-Helmholtz Instabilities (KHI), which have been studied at great length. For a step function profile in the velocity and constant densities across the shear layer, the growth rate is given by the velocity difference $k\Delta U$. If aligned with the flow, magnetic tension forces can stabilize against the KHI.

(3) The Thermal Instability (TI, Field 1965) rests on the balancing of heating and cooling processes in the ISM. The TI develops an isobaric condensation mode and an acoustic mode, which – under ISM-conditions – is mostly damped. The condensation mode's growth rate is independent of the wave length, however, since it is an isobaric mode, smaller perturbations will grow first (Burkert & Lin 2000). A lower growth scale is set by heat conduction, whose scale needs to be resolved (Koyama & Inutsuka 2004). The signature of the TI are fragmentation and clumping as long as the sound crossing time is smaller than the cooling time scale. The TI can drive turbulence in an otherwise quiescent medium, even continuously, if an episodic heating source is available (Kritsuk & Norman 2002a,b).

3 Numerical Method and Initial Conditions

The numerical method is based on the 2nd order BGK formalism (Prendergast & Xu 1993; Slyz & Prendergast 1999; Heitsch et al. 2004, Slyz et al. 2005), allowing control of viscosity and heat conduction. The statistical properties of the models are resolved with respect to grid resolution, viscosity and heat conduction, although the flow patterns change in detail — as to be expected in a turbulent environment (Heitsch et al. 2005, 2006). The linear resolution varies between 512 and 2048 cells. The heating and cooling rates are restricted to optically thin atomic lines following Wolfire et al. (1995), so that we are able to study the precursors of MCs up to the

point when they could form H_2 . Dust extinction becomes important above column densities of $N(\text{HI}) \approx 1.2 \times 10^{21} \text{cm}^{-2}$, which are reached only in the densest regions modeled. Thus, we use the unattenuated UV radiation field for grain heating (Wolfire et al. 1995), expecting substantial uncertainties in cooling rates only for the densest regions. The ionization degree is derived from a balance between ionization by cosmic rays and recombination, assuming that Ly α photons are directly reabsorbed.

Two opposing, uniform, identical flows in the x - y computational plane initially collide head-on at a sinusoidal interface with wave number $k_y = 1$ and amplitude Δ . The incoming flows are in thermal equilibrium. The system is thermally unstable for densities $1 \lesssim n \lesssim 10 \text{cm}^{-3}$. The cooling curve covers a density range of $10^{-2} \leq n \leq 10^3 \text{cm}^{-3}$ and a temperature range of $30 \leq T \leq 1.8 \times 10^4 \text{K}$. The box side length is 44pc. Thus, Coriolis forces from Galactic rotation are negligible. For an interface with $\Delta = 0$, a cold high-density slab devoid of inner structure would form. The onset of the dynamical instabilities thus can be controlled by varying the amplitude of the interface perturbation. This allows us to test turbulence generation under minimally favourable conditions.

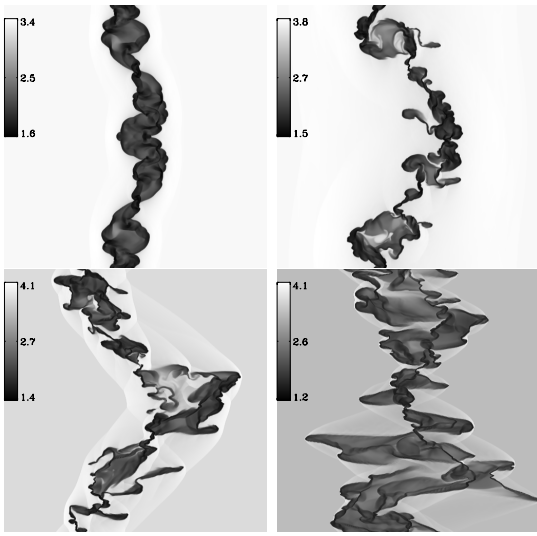


Figure 1: Temperature maps ($\log T$ in K) for models representative of the dominating instability (see text). From upper left to lower right, the models are dominated by TI, KHI, KHI+NTSI and NTSI respectively. Shown are models with 512^2 grid cells.

4 Results

4.1 Cloud Morphologies

Figure 1 shows stills of four representative models, each taken at approximately 12 Myrs after flow contact time. Each of the models is dominated by a different instability. High inflow densities and slow inflow speeds lead to TI-dominated slab-like structures (upper left). This comes closest to the case without any initial perturbation in the flow interface: a cold dense slab would form. Reducing the density but

keeping the inflow speed the same gives the dynamical instabilities time to act, since the cooling time scale increases. First, the KHI is excited because of the shear flows along the flank of the initial perturbation (upper right). Raising the inflow speed leads to increased x -momentum transport in the vertical, so that the NTSI starts to take over (lower left), and finally dominate the system (lower right). Obviously, colliding flows have no trouble at all to generate non-linear substructure inside the cold regions, and to lead to mixing of warm and cold phases.

4.2 Turbulence in the cold gas

Figure 2 (left) shows the line-of-sight velocity histogram for a sequence of models with increasing inflow Mach number (from Mach 1 to Mach 3). The histograms in

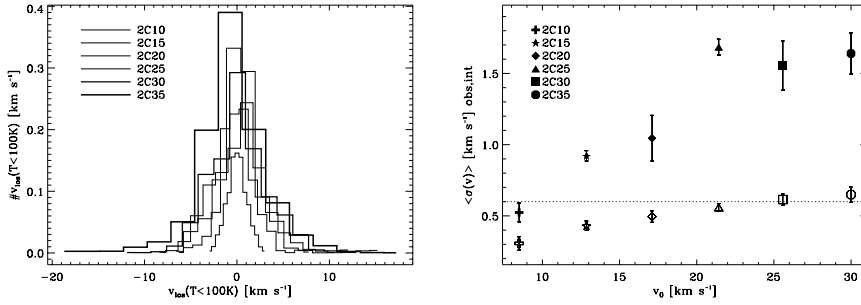


Figure 2: *Left:* Histogram of the line-of-sight velocities measured for a model sequence in Mach number (ranging from Mach 1 to Mach 3). Measurements are taken 12 Myrs after flow contact time. *Right:* “Observed” (solid symbols) and internal (open symbols) velocity dispersion for the same models as in the left panel (see text). While the “observed” Mach number is supersonic with respect to the cold gas, the internal Mach number is at most transsonic.

the left panel as well as the solid symbols in the right panel denote the “observed” velocity dispersion in the cold gas (at $T < 300$ K, derived from the density-weighted line-of-sight velocity in the cold gas). The open symbols, however, are derived from the internal dispersion of each coherent cold region, i.e. this measure gives information about the hydrodynamical state of the gas. While the “observed” velocity dispersion are consistent with observations, the internal values are at most transsonic, i.e. the “supersonic” turbulence in our models comes from motions of isolated cold gas regions with respect to each other. The term “supersonic” thus need not be an hydrodynamically accurate description of the gas.

Figure 3 shows the specific kinetic energy, split into solenoidal and compressible parts, for the whole domain (left panel), and the cold gas (right panel). Compressible modes dominate the full domain because of the highly compressible inflows, while the solenoidal modes dominate in the cold gas, i.e. the cold gas is moving close to solenoidally.

The power spectrum of the 3D model at Mach 2 corroborates these findings (Fig. 4). Clearly, the spectral index varies with the direction in which the spectrum is taken: Shown are the three linear spectra, taken along the inflow direction (α_x) and

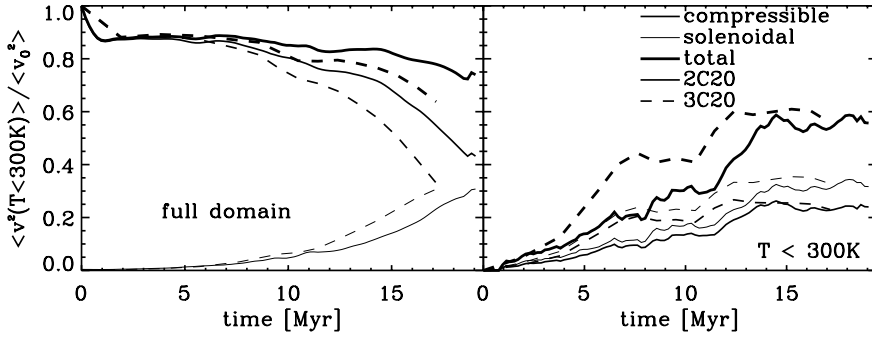


Figure 3: *Left:* Specific kinetic energy for the whole simulation domain for a model with Mach 2 inflow against time, split into compressible, solenoidal and total part. Solid lines stand for the 3D version, dashed lines for the 2D version. Compressible motions dominate because of the inflows. *Right:* Specific kinetic energy for the cold gas ($T < 300$ K) for the same models against time, split into compressible solenoidal and total part. Solenoidal motions dominate in the cold gas.

the transversal directions ($\alpha_{y,z}$). The spectral index $\alpha_x = -1.96$ is consistent with the Fourier transform of a step function, as to be expected since the strong decelerations along the x -direction effectively lead to a discontinuity in v^2 . The transversal directions α_y and α_z are consistent with a Kolmogorov spectrum, indicating fully developed turbulence. The lower spectrum (denoted by triangles and a corresponding slope $\alpha_c = -3.24$) shows the spherically averaged spectrum. Error bars denote errors of the mean. Within the errors, the slope is still consistent with a Kolmogorov spectrum of $-11/3$ in three dimensions.

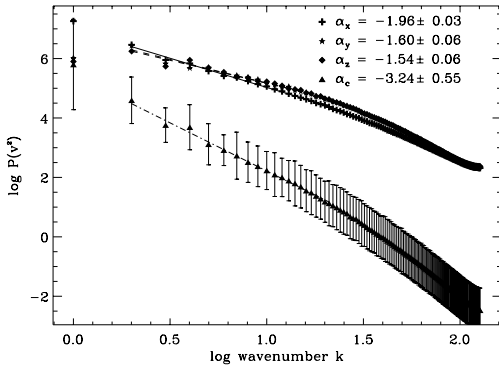


Figure 4: Specific kinetic energy spectrum for a 3D model, 12 Myrs after flow contact time. The linear spectral indices $\alpha_{x,y,z}$ refer to the coordinate directions, and α_c gives the index of the spherically averaged spectrum.

4.3 Precursors of Molecular Clouds

A crucial point in our analysis is whether the cold gas phase reaches conditions favorable for H_2 formation, and thus eventually for molecular clouds (so far we have

only been talking about the precursors of molecular clouds). Three criteria need to be met.

(1) The gas temperature has to drop below a threshold temperature for H_2 formation, which we set at $T_c = 300$ K (Cazaux et al. 2005). From Figure 5 we see that for reasonable inflow speeds a few $100M_\odot \text{ pc}^{-1}$ at $T < 300$ K accumulate within approximately 8 Myrs, i.e. this material would be available for H_2 formation – at least as far as the temperature is concerned.

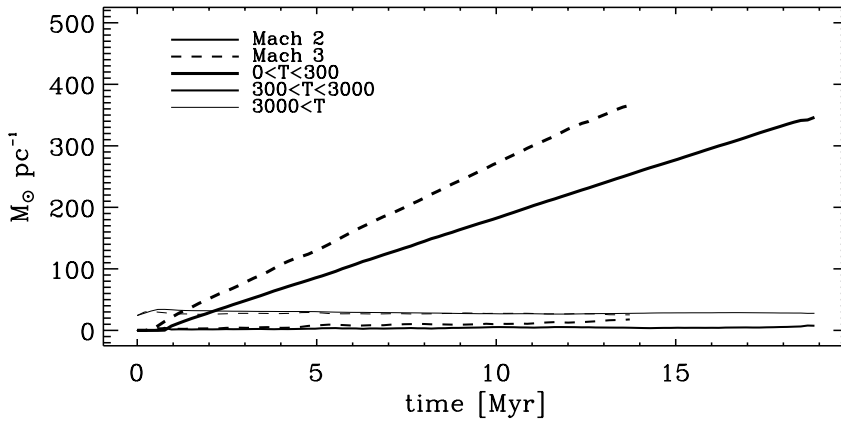


Figure 5: Mass content in the warm ($T > 3000$ K, thin lines), unstable ($300 < T < 3000$ K, medium lines) and cold ($T < 300$ K, thick lines) phase, for Mach 2 and Mach 3 inflows. Since the models shown are 2D, the mass unit is taken per length.

(2) The (now cold) gas has to stay cold “long” enough to allow for H_2 formation. Time estimates for H_2 formation vary. In their analysis of H_2 formation behind shock fronts, Bergin et al. (2004) quote timescales between 5 and 10 Myrs. Once H_2 exists, its further formation could well be a run-away process, since self-shielding is much more efficient than dust shielding. This means that the critical timescale is given by the onset of H_2 formation. A minimum requirement therefore is that the cold gas is not reheated during this timescale. To measure this, we followed the temperature history of the tracer particles and determined how long each particle stays cold. Figure 5 (left) is a histogram of the time intervals over which tracer particles have temperatures $T < 300$ K. Apart from a small fraction at short time intervals ΔT (these are particles at the rims of the cold regions), most of the particles stay cold for at least 6 Myrs. In fact, for most models, the cold gas parcels stay cold

(3) Finally, the cold, dense gas could be re-exposed to the ambient UV radiation field. H_2 formation requires a critical column density of $N(HI) \gtrsim 10^{21} \text{ cm}^{-2}$. This we can determine again with the tracer particles, resulting in Figure 6 (right), which combines the temperature criterion of Figure 6 (left) and the previously mentioned column density threshold. Dropping the temperature criterion does not affect the result. Thus the critical quantity is the shielding column density, not the temperature. In other words, once the gas enters the “cold” phase, its thermal timescale is short

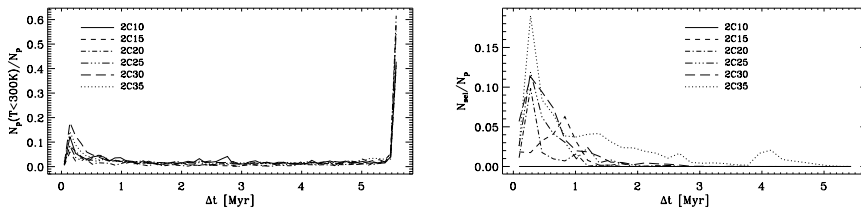


Figure 6: *Left:* Histogram of time intervals over which tracer particles stay at temperatures $T < 300$ K. Model sequence in Mach number. All models were run at $N = 512$. *Right:* Histogram of time intervals over which tracer particles “see” column densities $N > 10^{21} \text{ cm}^{-2}$ with respect to the ambient UV radiation field for the same models.

compared to the dynamical timescale, so that the gas stays isothermal. However, due to the constant re-structuring of the cloud, gas is repeatedly re-exposed to the UV radiation field. This is a direct consequence of the MCC’s highly dynamical nature. Note that Figure 6 (right) gives a pessimistic view: Once a small fraction of the particles have reached conditions beneficial for H_2 formation, self-shielding will set in.

5 Summary

Even for completely uniform inflows, we have shown that the combination of dynamical and thermal instabilities efficiently generates non-linear density perturbations that seed structure of eventual MCs. There is a direct correlation between the morphology of the resulting clouds and the dominating instability.

Linewidths reached in the cold gas are consistent with observed values of a few km s^{-1} – only a fraction of the inflow speed. The internal linewidths, however, are generally subsonic. While the linewidths are “supersonic” with respect to the cold gas, this is not necessarily a hydrodynamically accurate description of the cold gas.

Only a minor fraction of the gas is reheated after it has cooled down, however, most of the gas is re-exposed to the ambient radiation field, indicating strong mixing between warm and cold phases.

Although we set the physical regime for our models by adopting a cooling curve, we expect the mechanism to work on a variety of scales. The surface density of the cold gas should give us a rough estimate of the amount of stars forming later on. Even though the cold gas mass depends strongly on the turbulent evolution of the slab, it correlates strongly with the inflow momentum. In this sense, colliding flows not only could explain the rather quiescent star formation events as in Taurus, but would be a suitable model for generating star bursts in galaxy mergers.

References

- Audit, E., Hennebelle, P. 2005, A&A, 433, 1
- Ballesteros-Paredes, J., Hartmann, L., Vázquez-Semadeni, E. 1999, ApJ 527, 285
- Balsara, D. 1996, ApJ 465, 775
- Bergin, E. A., Hartmann, L. W., Raymond, J. C., Ballesteros-Paredes, J. 2004, ApJ 612, 921
- Burkert, A., Lin, D. N. C. 2000, ApJ, 537, 270
- Burkert, A. 2004, ASP Conf. Ser. 322: The Formation and Evolution of Massive Young Star Clusters, 322, 489
- Cazaux, S., Caselli, P., Tielens, A. G. G. M., Le Bourlot, J., Walmsley, M. 2005, J. Phys., 6, 155
- Elmegreen, B. G., Falgarone, E. 1996, ApJ 471, 816
- Elmegreen, B. G. 2000, ApJ, 530, 277
- Elmegreen, B. G., Scalo, J. 2004, ARAA 42, 211
- Falgarone, E., Philips, T. G. 1990, ApJ 359, 344
- Field, G. B. 1965, ApJ, 142, 531
- Hartmann, L., Ballesteros-Paredes, J., Bergin, E. A. 2001, ApJ 562, 852
- Hartmann, L. 2002, ApJ 578, 914
- Heitsch, F., Burkert, A. 2002, ASP Conf. Ser. 285: Modes of Star Formation and the Origin of Field Populations, 285, 13
- Heitsch, F., Burkert, A., Hartmann, L., Slyz, A. D., Devriendt, J. E. G. 2005, ApJL 633, L113
- Heitsch, F., Slyz, A. D., Devriendt, J. E. G., Hartmann, L., Burkert, A. 2006, *in preparation*
- Heitsch, F., Zweibel, E. G., Slyz, A. D., & Devriendt, J. E. G. 2004, ApJ, 603, 165
- Hennebelle, P., Pérault, M. 1999, A&A 351, 309
- Hennebelle, P., Pérault, M. 2000, A&A 359, 1124
- Hennebelle, P., Whitworth, A. P., Gladwin, P. P., & André, P. 2003, MNRAS 340, 870
- Hennebelle, P., Whitworth, A. P., Cha, S.-H., & Goodwin, S. P. 2004, MNRAS 348, 687
- Hueckstaedt, R. M. 2003, New Ast. 8, 295
- Hunter Jr., J. H., Sandford II, M. T., Whitaker, R., Klein, R.I. 1986, ApJ 305, 309
- Klein, R. I., Woods, D. T. 1998, ApJ 497, 777
- Koyama, H., & Inutsuka, S. 2002, ApJ 532, 980
- Koyama, H., & Inutsuka, S. 2002, ApJL 564, L97
- Koyama, H., & Inutsuka, S. 2004, ApJL 602, L25
- Koyama, H., & Inutsuka, S. 2004, RMxAC 22, 26
- Kritsuk, A. G., & Norman, M. L. 2002, ApJL 569, L127
- Kritsuk, A. G., & Norman, M. L. 2002, ApJL 580, L51
- Mac Low, M.-M., & Klessen, R. S. 2004, Reviews of Modern Physics 76, 125
- Prendergast, K. H., Xu, K., 1993, J. Comp. Phys., 109, 53

- Slyz, A. D., Prendergast, K. H. 1999, A&AS, 139, 199
- Slyz, A. D., Devriendt, J. E. G., Bryan, G., & Silk, J. 2005, MNRAS, 356, 737
- Stutzki, J., Bensch, F., Heithausen, A., Ossenkopf, V., Zielinsky, M. 1998, A&A 336, 697
- Walder, R., Folini, D. 1998, ApSS, 260, 215
- Walder, R., Folini, D. 2000, ApSS, 274, 343
- Williams, J. P., Blitz, L., McKee, C. F. 2000, Protostars and Planets IV, 97
- Wolfire, M. G., Hollenbach, D., McKee, C. F., Tielens, A. G. G. M., Bakes, E. L. O. 1995, ApJ, 443, 152